CONTRACTOR REPORT

SAND99-0748
Unlimited Release

Random and Uniform Reactive Ion Etching Texturing of Si

Saleem H. Zaidi
Center for High Technology Materials
1313 Goddard SE
University of New Mexico
Albuquerque, NM 87106

Prepared by
Sandia National Laboratories
Albuquerque, New Mexico 87185 and Livermore, California 94550

Sandia is a multiprogram laboratory operated by Sandia Corporation, a Lockheed Martin Company, for the United States Department of Energy under Contract DE-AC04-94AL85000.

Approved for public release; distribution is unlimited.

Printed April 1999

Sandia National Laboratories

Issued by Sandia National Laboratories, operated for the United States Department of Energy by Sandia Corporation.

NOTICE: This report was prepared as an account of work sponsored by an agency of the United States Government. Neither the United States Government, nor any agency thereof, nor any of their employees, nor any of their contractors, subcontractors, or their employees, make any warranty, express or implied, or assume any legal liability or responsibility for the accuracy, completeness, or usefulness of any information, apparatus, product, or process disclosed, or represent that its use would not infringe privately owned rights. Reference herein to any specific commercial product, process, or service by trade name, trademark, manufacturer, or otherwise, does not necessarily constitute or imply its endorsement, recommendation, or favoring by the United States Government, any agency thereof, or any of their contractors or subcontractors. The views and opinions expressed herein do not necessarily state or reflect those of the United States Government, any agency thereof, or any of their contractors.

Printed in the United States of America. This report has been reproduced directly from the best available copy.

Available to DOE and DOE contractors from
Office of Scientific and Technical Information
P.O. Box 62
Oak Ridge, TN 37831

Prices available from (615) 576-8401, FTS 626-8401

Available to the public from
National Technical Information Service
U.S. Department of Commerce
5285 Port Royal Rd
Springfield, VA 22161

NTIS price codes
Printed copy: A03
Microfiche copy: A01

SAND99-0748
Unlimited Release
Printed April 1999

Random and Uniform Reactive Ion Etching Texturing of Si

Saleem H. Zaidi
Center for High Technology Materials
1313 Goddard SE
University of New Mexico
Albuquerque, NM 87106

Sandia Contract – BB-7211

ABSTRACT

The performance of a solar cell is critically dependent on absorption of incident photons and their conversion into electrical current. This report describes research efforts that have been directed toward the use of nanoscale surface texturing techniques to enhance light absorption in Si. This effort has been divided into two approaches. The first is to use plasma-etching to produce random texturization on multicrystalline Si cells for terrestrial use, since multicrystalline Si cannot be economically textured in any other way. The second approach is to use interference lithography and plasma-etching to produce gettering structures on Si cells for use in space, so that long-wavelength light can be absorbed close to the junction and make the cells more resistant to cosmic radiation damage.

Contents

1. Introduction 1

2. Randomly Textured Nanoscale Surfaces 2

3. Periodically Textured Nanoscale Surfaces 6

4. Nanoscale Textured Si Solar Cells 11

5. Discussion of results and Future Work 13

6. References 16

1. Introduction

The performance of a solar cell is critically dependent on absorption of incident photons, and their conversion into electrical current. Significant research efforts have been invested aimed at improving both aspects of solar cell devices. This report concentrates on surface texturing techniques resulting in enhancing light absorption in Si. Si has a large absorption coefficient in the visible, albeit, it also has a high reflection coefficient [1]. Reflection losses are reduced by applying anti-reflection (AR) films to a Si surface [2]. AR films have a resonant structure that limits their effectiveness to a narrow range of angles and wavelengths. An effective alternative has been geometrical texturing [3] of a Si surface combined with appropriate AR film stack. Since, Si is an indirect band gap semiconductor with weak absorption near the band edge, geometrical texturing schemes are basically designed to improve absorption near the bandgap. The light trapping concept is based on geometrical optics considerations using the fact that beyond the critical angle of incidence $\theta_c=\sin^{-1}(1/n)$ light is totally internally reflected, for Si, $\theta_c \sim 16°$ in IR (~ 0.8-1.1 μm) spectral range. Light inside this cone escapes from the semiconductor, rest is totally internally reflected. Maskless pyramidal texturing [3] of front and back surfaces of a solar cell helps randomize the direction of light within the substrate so as to minimize its escape from the cell. Enhanced absorption is achieved during several passes through the cell.

An alternative approach to light trapping has also been investigated, and is better understood by a brief review of statistical mechanics considerations. In a weakly absorptive medium, the number density of photons absorbed at a given frequency ω is proportional to the product of four factors $u(\omega)*a*(c/n)*(d^3k/d\omega)$, where $u(w)=[(\exp(h\omega/kT)-1)]^{-1}$ is the Bose occupation number for solar radiation, a is the absorption coefficient of the material, c is the velocity of light in vacuum, n is material refractive index, k is the wave vector of light, and $1/n\ d^3k/d\omega$ is the effective density of states $\rho(w)$ for absorption. In an isotropic medium, a photon state is represented by a plane wave of definite polarization and propagation vector. The number density of these states is proportional to $4\pi k^2$, where $k=2\pi/\lambda$. In an isotropic medium of refractive index n, $k=n*k$ so that the density of states in a medium is larger by a factor of n^2. These extra photon states can be visualized as light rays travelling in an optically dense medium at angles > θ_c. If these internally reflected rays are fully populated by scattering from random surfaces, then absorption is enhanced by a factor of n^2 [4]. In a detailed statistical analysis, Yablonovitch has shown that effective absorption can be enhanced by as much as a factor of $4n^2$ over a planar sheet [5]. However, in order to reach this statistical mechanics limit, surface texture must fully randomize incident light to fill internal optical phase space. Deckman et al. [6] have demonstrated that optimum random textures have dimensions slightly larger than the wavelength of light in the material. If the lateral dimensions of the microstructure are too large, light is specularly reflected reducing internal randomization, and if the lateral dimensions are much smaller than the wavelength of light, scattering is not effective, which again reduces internal randomization. Therefore, in order to optimize absorption, a precise balance between randomness and microstructure dimensions has to be maintained. Thus, in this physical optics approach, the enhanced absorption is expected to achieved predominantly by light trapping in nanoscale textures, and the requirement of multiple passes through the cell as in the case of geometrical optics texturing is not critical.

If instead of a random surface, a periodically textured surface such as a grating is used, the absorption may be enhanced beyond this statistical limit. The basic physics of this approach has been explained by Ping Sheng et al. [4] in terms of a rough analogy between interactions of photons with a periodic structure, and interactions of electrons with a periodic lattice in a crystal. The effect of the periodic structure is to create peaks in the particle density of states at one set of frequencies at the expense of gaps at the others keeping total integrated number of states fixed. By choosing grating parameters such that the gap in $\rho(\omega)$ falls below the absorption edge, peaks in $\rho(\omega)$ above it, photon

states from non-absorbing region are transferred to the absorbing region. In this way, $\rho(\omega)$ can be enhanced beyond the statistical limit.

Rest of this report is divided into following sections: in section 2 we characterize randomly textured surfaces, section 3 presents optical analysis of periodic structures, solar cell device results are presented in section 4, section 5 discusses results and proposed future work, and finally references are in section 6.

2. Randomly Textured Nanoscale Surfaces

In section 1 three techniques were discussed for reducing Si surface reflection. Light trapping by inverted pyramidal structures has been extensively used in Si solar cell manufacturing. These structures are wet-chemically etched on a polished surface of (100) orientation. This texturing scheme suffers from the following disadvantages:

a) wet-etching is not effective in multi-crystalline Si solar cells,
b) the structural dimensions are ~ few micrometers limiting applicability to thick-film solar cells only,
c) absorption in IR region, is achieved by several passes through the cell thus necessitating application of high quality material, and
d) radiation damage in the bulk of the material (for space solar cells) reduces minority carrier diffusion lengths thus enhanced absorption away from the junction does not contribute to photo-current.

A random texturing scheme independent of these constraints is expected to improve Si solar cell performance. We have developed random texturing processes applicable to both polished and multi-crystalline surfaces [7]. The reactive ion etching (RIE) texturing processes are extensively used in IC manufacturing, and provide a unique capability for precise etching of nanoscale structures [8]. The random nanoscale texturing for reduced reflection was first reported by Gittleman et al. [9] in a maskless RIE process. Si reflection was measured to be less than 0.001 % in the visible region. These structures had lateral dimensions of ~ 100-300 nm, and depths ~ 0-2000 nm. Similar structures formed by reactive ion etching were also reported by Craighead et al. [10] in thin Si films. More recently, Jansen et al. [11] have reported on RIE schemes to form a black Si surface consisting of high aspect ratio nanoscale columnar structures. It is generally recognized that reactive ion etching of Si can yield almost black surfaces, however, no systematic research effort has been directed at large area fabrication of these surfaces.

We have investigated random texturing of Si aimed at reduced Si reflection in the visible to IR spectral regions. The reactive ion etching experiments were carried out at room temperature in a Techniques PEII-A parallel plate reactor using SF_6/O_2 based plasma chemistry. Optimum random texturing parameters were obtained at ~ 50 W RF power at a pressure of ~ 180 mTorr, and SF_6/O_2 flow ratio of ~ 1, etching rate under these conditions was ~ 0.1-μm / min. In our initial experiments, small (~ 1-2 cm) Si samples were mounted on an Al substrate inside the RIE chamber. Figure 1 shows normal incidence spectral reflectance of Si surface as a function of the etching time, for comparison, reflection from a polished Si surface under identical conditions had been normalized to unity, and same normalization factor was applied to reflection data from the etched surfaces. From Fig. 1, it is seen that reflection reduction achieved after 15-minutes of etching (at least ~1.5-μm thick Si). The etched surfaces show almost zero reflection in the visible and only slightly higher reflection in the IR region. At λ ~ 600-nm, the reflection from the 30-min etched sample is reduced by a factor of 85 relative to bare Si. Assuming 0.33 absolute Si reflectance, this represents absolute Si reflection of ~ 0.004 without applying any anti-reflection films. The 15-30 min RIE samples appear almost black at normal incidence, and at

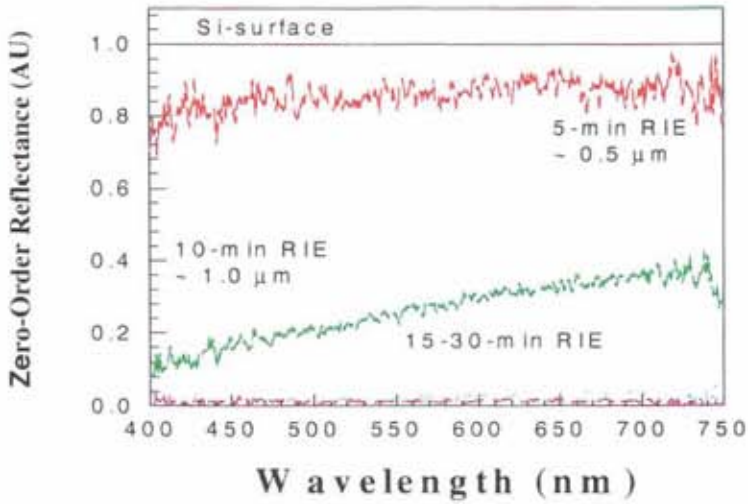

Figure 1 Normal incidence spectral reflectance from randomly etched Si structures.

large incident angles show slightly higher bluish reflectance. We have carried out scanning electron microscope (SEM) investigation of these randomly etched surfaces. It is seen that the absorptive texture consists of densely packed, random inverted pyramids, with lateral dimensions of ~ 100-500 nm, and depths ~ 0-1000 nm.

For photovoltaic device applications large area application of these random texturing schemes is desirable. We investigated texturing of 4" wafers under identical conditions. The reactive ion etching processes failed to form absorptive surface structure. From visual inspection of 4" wafers, edges appeared to have strong dark texture, whereas the center did not exhibit any texture. This suggested that during RIE process, microscopic Al particles are sputtered and deposited on Si to act as random etch masks. These Al particles don't have enough energy to travel to the wafer center so that no appreciable texture is developed. In order to verify this, we etched two Si samples at the same time. One sample was mounted on Al, other on the RIE chamber surface. After 30 minutes of etching, both samples were removed from the chamber. The sample on Al holder had developed a black texture, whereas the sample without Al base did not exhibit a significant texture. Figure 2 shows normal incidence spectral reflectance measurements on these two samples, for comparison Si reflectance under identical conditions normalized to unity is also shown. It is seen that sample on Al substrate shows broadband reduced reflection similar to that observed in Fig. 1, whereas the Si sample without Al base shows only ~ 40 % reduction in reflection in comparison with polished Si. Figures 3 & 4 show SEM pictures of texture on absorptive and non-absorptive samples. It is seen that non-absorptive texture consists of random distribution of 10-50 nm lateral features without any significant depth. The absorptive structure has a random distribution of pyramidal structures with typical dimensions ~ 100-1000 nm, and depths ~ 1000 nm. Comparison of feature dimensions in Figs. 3 & 4 shows that reduced reflection is accomplished by high aspect ratio nanoscale (~ 100-500 nm) feature sizes. Si refractive index in the UV-to-IR range varies from ~ 6.86 to 3.54 [1] so that λ/n is ~ 50-300 nm inside the semiconductor material. These lateral dimensions are large enough to trap light inside these random nano-structures leading to enhanced absorption and broadband reduced reflection. For 10-50 nm lateral features (Fig. 4), the dimensions are too small for effective light trapping, and hence no significant reduction in reflection is observed (Fig. 2).

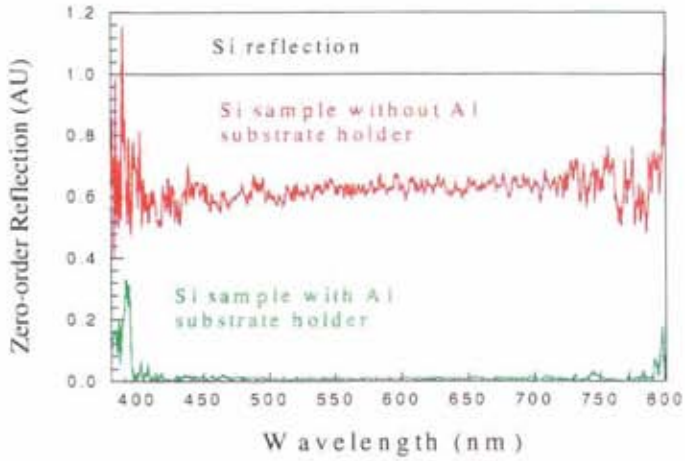

Figure 2 Normal incidence spectral reflectance from randomly etched Si structures without and without Al holders.

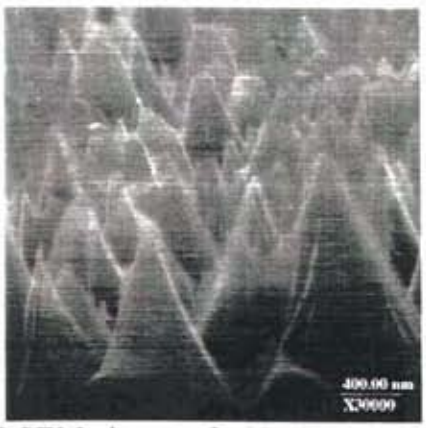

Figure 3 SEM picture of a black Si RIE-textured surface.

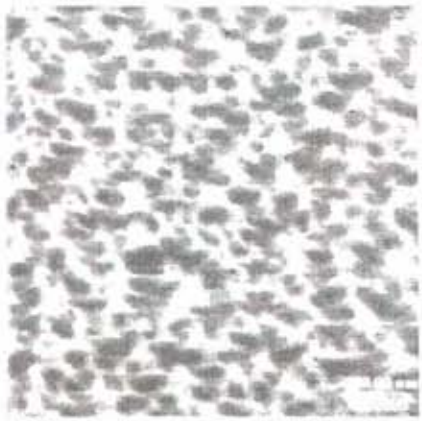

Figure 4 SEM picture of a lightly absorptive Si RIE-textured surface.

2.a Maskless Nanoscale Texturing of Si

We have demonstrated that Si absorptive texture in an RIE chamber is a result of micro-masking by sputtered Al particles. Small Al particles can be identified at the top of the pyramids in Fig. 3. For large area texturing, an alternate approach is required that can deposit a random etch mask on a single, or multi-crystalline surface. One such approach is natural lithography developed by Deckman et al. [12]. In this approach, sub-μm (~ 0.1-0.8 μm) silica spherical particles are spin-coated onto the semiconductor surface, and act as etch RIE masks. We have investigated this method, and had difficulty in forming a uniform coverage of silica particles, more work needs to be done in understanding the chemistry between silica particles and Si surface. We have been able to develop an alternate texturing scheme that is effective in forming black Si surfaces. This new method takes advantage of differential etching rates of oxide and Si in SF_6/O_2 gas plasma, i.e., Si etching is much faster than SiO_2. A thick (~ 0.6 μm) TEOS oxide grown on a Si surface is used as the etch mask. As the oxide is etched off and SiO_2/Si interface reached, microscopic oxide particles act as etch masks to create nanoscale surface texturing in Si. Figure 5 shows SEM pictures of the transition region, fine (~ 10-30 nm) SiO_2 particles are seen that have acted as etch masks in forming the high aspect ratio, vertical sidewall random texture in Si.

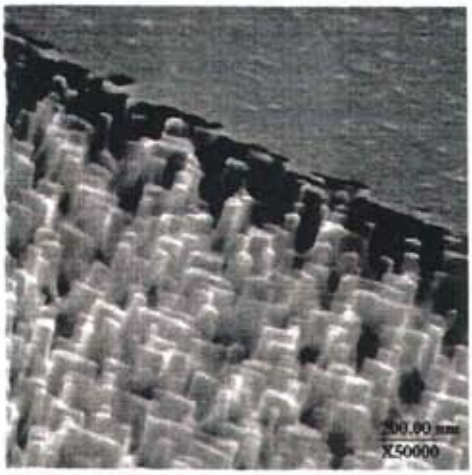

Figure 5 SEM picture of texturing at SiO_2/Si interface.

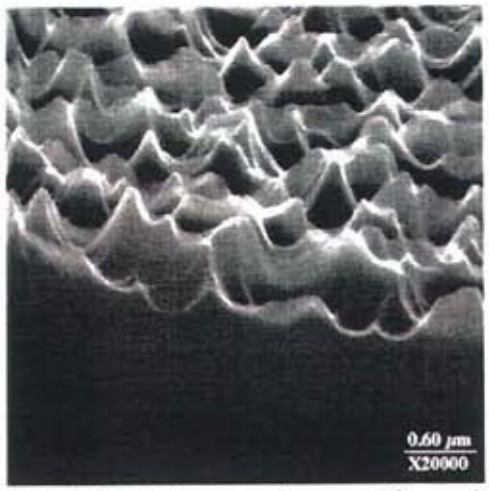

Figure 6 SEM picture of texture formed by additional etching of columnar structure in Fig. 5.

Figure 6 shows pyramidal structures etched in Si following additional etching of vertical high aspect ratio structures of Fig. 5. In comparison with Fig. 5, surface reflection is substantially reduced by the texture of Fig. 6. The etching results of Figs. 5-6 demonstrate the possibility of controlling random texturing process, i.e., from columnar to pyramidal profiles. This may be of interest for wavelength tuneability of photodetectors in the UV-IR spectral regions. We have investigated various surface textures to correlate feature size with reflection. Figure 7 shows hemispherical reflectance measurements carried out at Sandia Laboratories of two randomly textured surfaces made from the same substrate material, for comparison reflectance from polished Si under identical conditions is also plotted. The reflection plot identified as texture # 1 (black line) shows significantly reduced reflection (~ 5-10 %) in the UV-Visible spectral range, the texture # 2 (red line) shows reduced reflection ~ 15 % in the same region. However, in the 1100-1200-nm region, texture # 2 shows reduced reflection in comparison with texture # 1. The

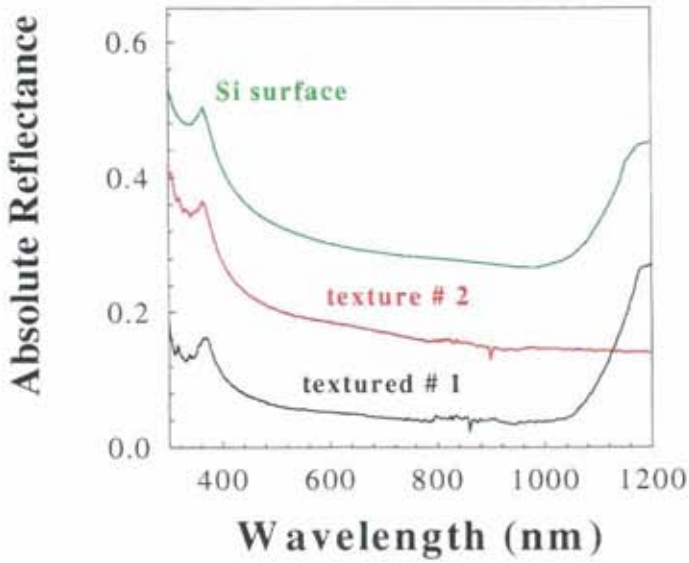

Figure 7 Hemispherical spectral reflectance from two randomly etched Si surfaces.

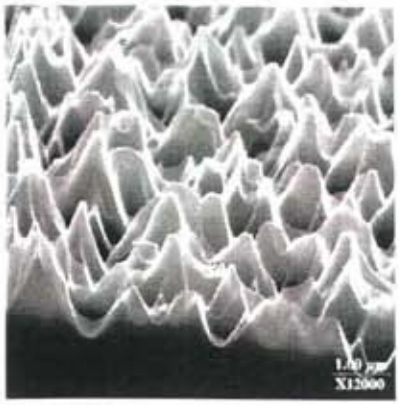

Figure 8 SEM picture of the texture # 1 Si surface in Fig.7, SEM scale is 1.0 μm.

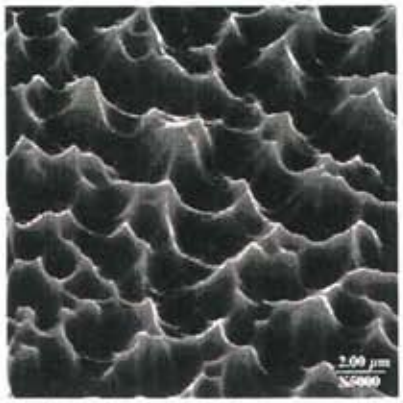

Figure 9 SEM picture of the texture # 2 Si RIE-textured surface in Fig.7, SEM scale is 2.0 μm.

surface profiles corresponding to textures # 1 & 2 are shown in Figs. 8 & 9 respectively. The lowest UV-Visible reflection is exhibited by fine (100-500 nm), high aspect-ratio random feature sizes. At larger (~ 1.0-2.0 μm) dimensions (Fig. 9), light trapping in the UV-Visible spectral regions is not as effective, however, this texture is more effective in light trapping at longer wavelengths (~ 1.1-1.2 μm) in comparison with the finer texture of Fig. 8.

3. Periodically Textured Nanoscale Surfaces

Randomly textured nanoscale surfaces exhibit broad band absorptive behavior. In order to achieve narrow band spectral response, uniform structures are required. High aspect ratio, nanoscale linewidth sub-μm period grating structures offer significant potential in tailoring reflectance profile to a desired spectral range [13]. Interferometric lithography (IL) provides an inexpensive method of fabrication of nanoscale periodic structures over large areas [14]. Interference between two coherent laser beams produces a simple periodic pattern with period, $d=\lambda/2\sin\theta$, where λ is the wavelength of the exposing laser beam, and 2θ is the angle between two intersecting laser beams. Typically grating structures are first formed in positive photoresist followed by pattern transfer to the substrate using wet, or dry etching techniques. Using IL techniques, we have investigated optical properties of 1-D Si gratings with periods varying from ~ 0.2-1.0 μm, linewidths ~ 0.02-0.5 μm, and depths ~ 0.5-1.0 μm [13]. The normal incidence spectral reflectance of gratings at ~ 1.0-μm depth was observed to have a strong dependence on linewidth and incident light polarization. Figure 10 shows hemispherical reflectance of three grating structures with periods ~ 1.0, 0.5, and 0.3 μm, and depths ~ 1.0 μm, for comparison reflectance from polished Si surface under identical conditions is also plotted. As the period decreases, linewidths also decrease: for the three gratings measured, linewidths were ~ 0.33, 0.13, and 0.05 μm respectively. Figure 11 shows SEM pictures of three grating structures showing high aspect ratio, rectangular profiles. From reflection measurements in Fig. 10 it is seen that 1.0-μm (linewidth ~ 0.33 μm) period grating (black line) does not exhibit reduced reflection. A reflection dip at $\lambda \sim 0.92$ μm is observed which approximately corresponds to $\theta_{\pm1} \sim 90°$ in air, i.e., ±1-diffraction orders are parallel to the surface. Due to large refractive index of Si in the UV-Visible spectral range, at this period, there are a large number of diffraction orders inside Si. Some of the dips in the reflectance in 400-800-nm spectral range probably correspond to higher order diffraction orders becoming parallel to surface inside Si. For 500-nm period (red line), reflection is substantially reduced in comparison with bare Si surface. A pronounced reflectance dip at $\lambda \sim 500$ nm probably corresponds to $\theta_{\pm1} \sim 90°$, the second dip at ~ 900 nm appears to correspond to $\theta_{\pm2} \sim 90°$ inside Si. For the 300-nm period (yellow line), the reflection dip at $\lambda \sim$

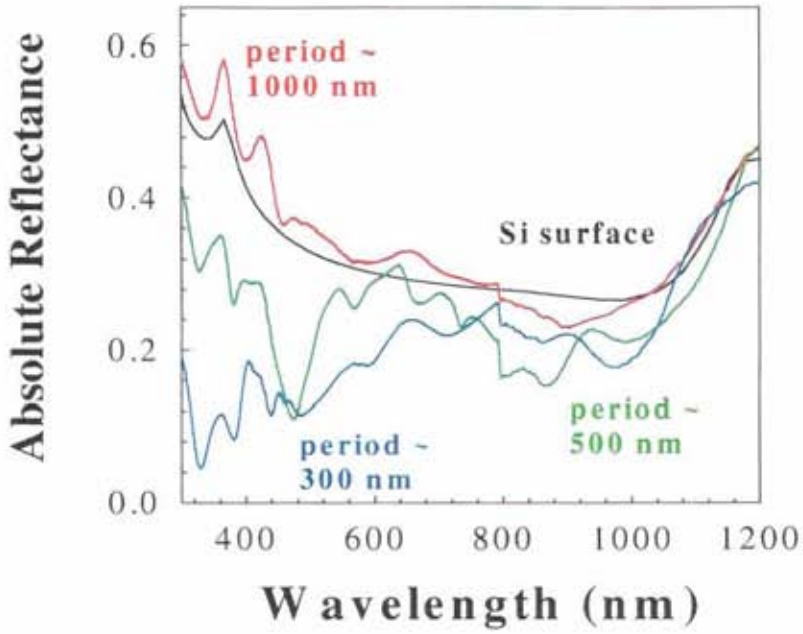

Figure 10 Hemispherical spectral reflectance from three Si 1-D grating surfaces.

period ~ 1000 nm, linewidth ~ 330 nm

period ~ 500 nm, linewidth ~ 130 nm

period ~ 300 nm, linewidth ~ 50 nm

Figure 11 Hemispherical spectral reflectance from three Si 1-D grating surfaces.

320 nm probably corresponds to $\theta_{\pm 1} \sim 90°$ in air. The reflectance dip at $\lambda \sim 1000$ nm probably corresponds to $\theta_{\pm 1} \sim 90°$ in Si. These measurements demonstrate a trend of reducing reflection as both period and linewidth are reduced. For linewidths ≈ 50 nm, or smaller, reflection in the IR region of the spectra starts to approach polished Si. These diffraction, and light-trapping related resonance effects are expected to be more pronounced for either 2-D structures, or for polarized incident light. Also, a better correlation of reflection with linewidth can be established by reducing linewidths while keeping period fixed. We have carried out extensive normal incidence measurements of 1-D structures, and have observed polarization-dependent, narrow-band spectral response. Figure 12 shows an example of the spectral response of the 1000-nm period structure shown in Fig. 11. A periodic polarization-dependent spectral reflectance variation is observed. We have observed this spectral reflectance behavior for grating linewidths down to ~ 50 nm, below which a broad band reduced reflectance is seen for TM-polarized light, and a monotonically increasing reflectance from UV-IR region for TE-polarized light.

We have also investigated spectral reflectance response of triangular profile gratings. The triangular profile is much closer to the randomly textured profiles shown earlier. Figure 13 shows

hemispherical spectral reflectance measurements of two 1-D grating structures, for comparison, reflection from bare and randomly textured Si surface is also shown. It is seen that these surfaces exhibit broadband anti-reflection behavior, and overall reflectance decreases as grating period and linewidths

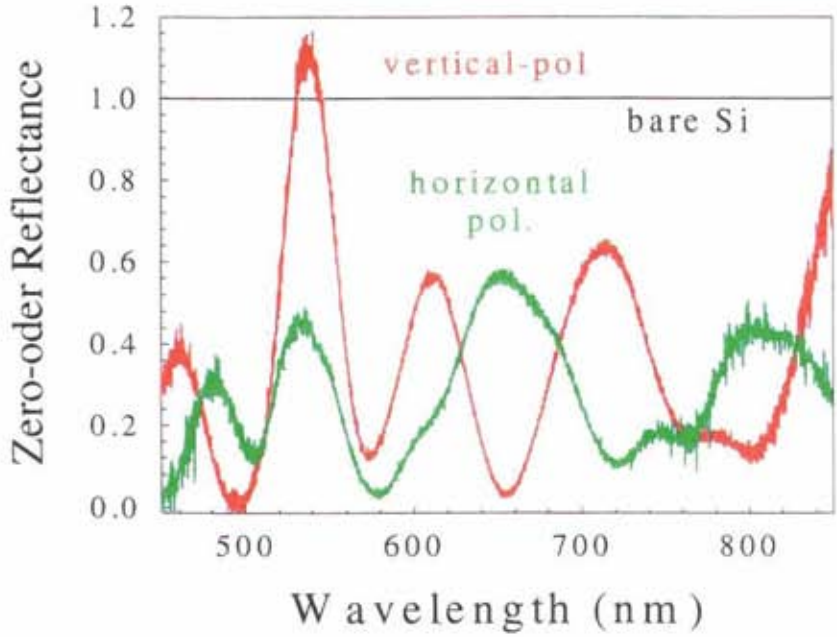

Figure 12 Normalized, normal incidence spectral reflectance from the 1000-nm period, 330-nm linewidth 1-D grating shown in Fig. 11, vertical and horizontal polarizations refer to E-field parallel and perpendicular to grating lines.

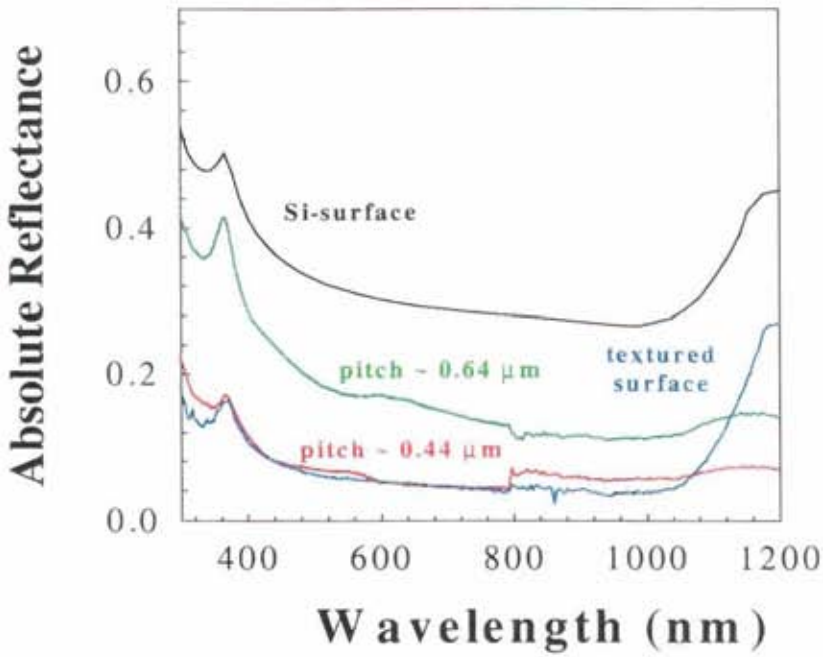

Figure 13 Hemispherical spectral reflectance from three Si 1-D triangular-profiled grating surfaces.

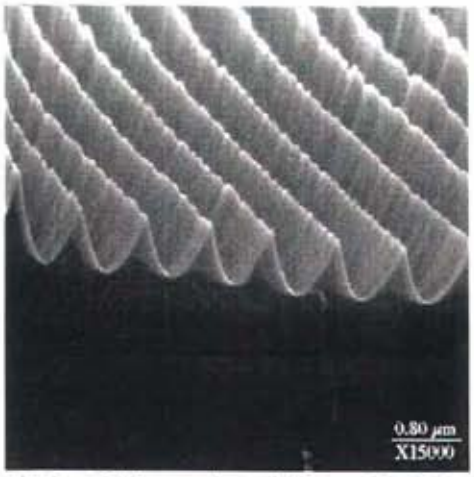

period ~ 640 nm, linewidth ~ 60-300 nm

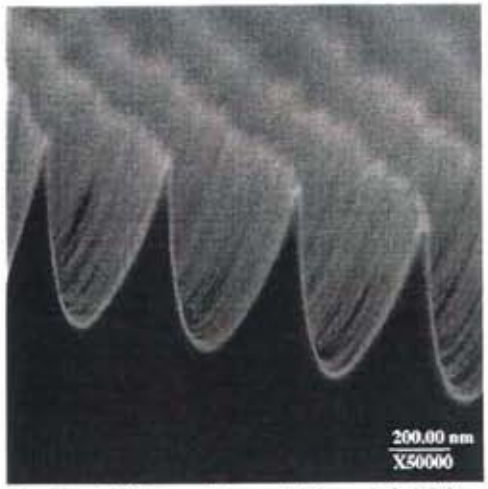

period ~ 440 nm, linewidth ~ 15-100 nm

Figure 14 SEM pictures of highly absorptive Si 1-D gratings at ~ 600-nm depth.

are reduced from 0.64 to 0.44 μm. Considering that these are 1-D structures, and incident light is non-polarized, we expect additional reflection reduction for 2-D grating structures. Figure 14 above shows SEM pictures of the gratings used for measurements in Fig. 13. The 0.64-μm period grating has a depth of ~ 0.6 μm, linewidth varies from ~ 60 nm at the top to ~ 300 nm at half grating depth. The 0.44-μm period grating has a depth of ~ 0.6 μm, and linewidth varies from ~ 15 nm at the top to ~ 100 nm at half grating depth. Thus, it appears that reflection is reduced more effectively by linewidths in ~ 20-100 nm linewidth range. In addition, tapered triangular profiles show a broadband anti-reflection behavior in contrast with the spectrally selective reflection of rectangular profiles.

3.a Enhanced Absorption in Grating Structures

We have seen that grating profiles can be tailored for either narrow-band, or broad-band anti-reflection behavior. For space solar cell application, it is desirable that light in the 800-1200-nm range be absorbed close to the surface. It is therefore important to determine the physical mechanisms responsible for reduced reflection. Reduced reflection can be accounted by either one of the four mechanisms described below:

a) Grating profile behaves as an anti-reflection film,
b) Grating profile traps light due to λ/n type of resonant lateral dimensions,
c) Grating profile couples light into diffraction orders, and
d) A combination of one or more mechanisms described above.

Absorption measurements can help understand underlying physical mechanisms. Absorption in thin Si films can be measured in both visible and IR range by carrying out reflection and transmission measurements. In order to carry out these measurements, we used Si-on-Sapphire configuration (SOS). These SOS wafers are commercially available, and had a 1.6-μm thick crystalline Si film on top of a thick sapphire substrates. Using IL, 1-D gratings were etched in the top Si surface at periods 1.0, 0.5, and 0.3 μm. Absorption in each grating was measured by taking the difference of reflection and transmission, i.e., absorption, A=1-T-R, notice that R, T also include diffraction orders. Figure 15 shows the results of hemispherical absorption measurements, for comparison, absorption calculated for 1.6-μm

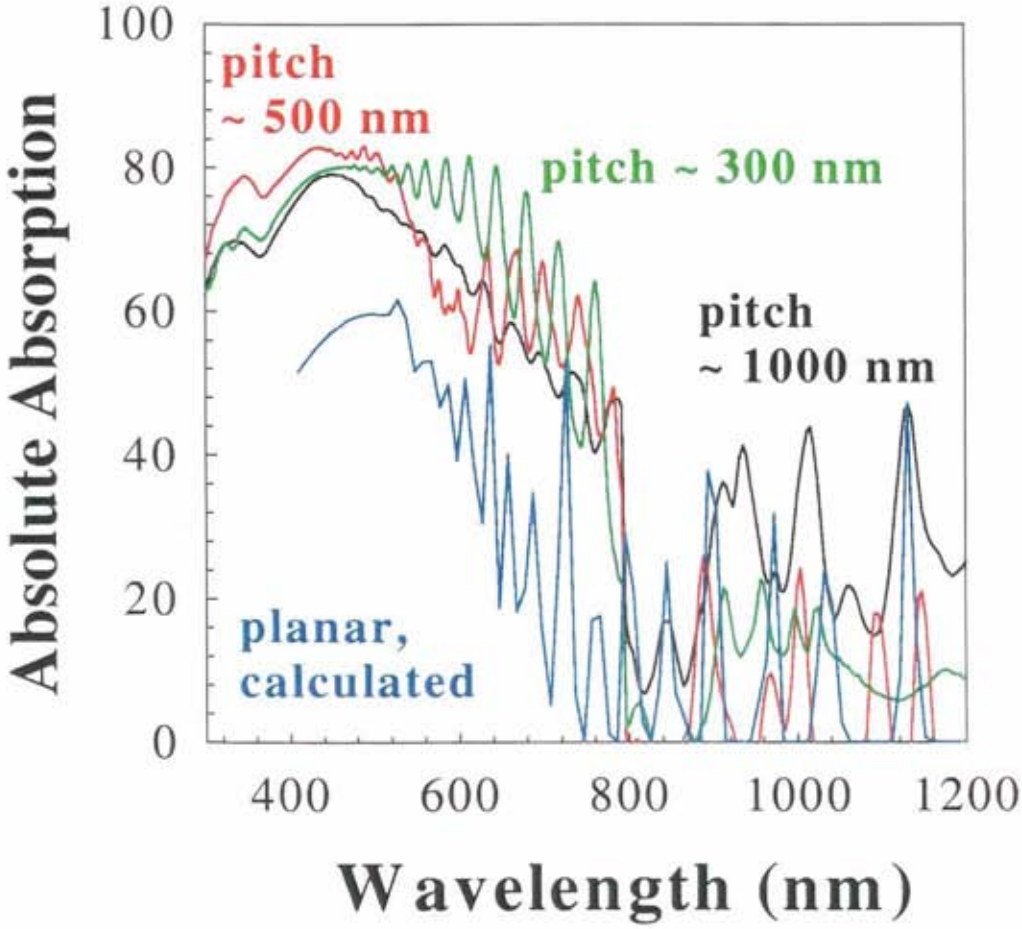

Figure 15 Hemispherical absorption in 1-D grating structures in SOS configuration.

thick Si film on sapphire is also plotted. The periodic variation in intensity is due to the thin-film waveguide structure. Absorption measurements demonstrate an enhancement in the UV-Visible spectral region for 0.3 and 0.5-μm period textures, at 1.0-μm period, enhanced absorption is seen in the 800-1200 nm region. For the 300-nm period (green line), the first order at $\lambda \sim 300$ nm becomes evanescent in air, which should have significantly increased absorption. This lack of absorption enhancement suggests that the grating profile did not efficiently couple light in the first diffraction order. Increased absorption at $\lambda \sim 600$ nm for the 300-nm period is due to the second diffraction order becoming evanescent inside Si, similarly enhancement at $\lambda \sim 1000$ nm appears to be due to first diffraction order becoming evanescent inside Si. At 500-nm period (red line), absorption enhancement is seen at $\lambda \sim 400$-500 nm region possibly due to first diffraction order in air becoming evanescent. At 1000-nm period (black line), absorption enhancement in the $\lambda \sim 900$-1200 nm region appears to be due to first diffraction order in air becoming evanescent.

These measurements demonstrate significant selective absorption enhancement due to 1-D grating structures. Since, the incident light was non-polarized, the enhancement is expected to be at least twice as much for 2-D grating structures. Finally, optimization of grating profiles would further enhance absorption.

4. Nanoscale Textured Solar Cell Devices

We have applied random and periodic texturing schemes to multi-crystalline and single crystalline polished surfaces. The random texturing process was applied to Solarex mc-Si solar cell devices. The texturing was done using a PECVD oxide as an etch mask. This oxide is not as effective as TEOS oxide in fabrication of highly absorptive structures. The measurements on etched devices are shown in table 1 below. It is seen that for the three RIE-textured cells, ISC was increased by ~ 2 % over the control cells, although overall efficiency and VOC were reduced. This preliminary measurement demonstrates applicability to mc-Si, and suggests that process optimization will result in improved performance.

Table-1
Sandia RIE Texture Process / Solarex mc-Si solar Cells

CELL	EFFIC	PMAX	ISC	VOC	FF	R-SERIES	R-SHUNT	N FACTOR
101 Control	12.33	1.603	3.800	570	74.0	9.5	222	1.210
102 Control	12.38	1.609	3.816	570	73.9	9.0	91	1.197
103 RIE	10.44	1.357	3.893	544	64.1	6.9	13	2.197
104 RIE	12.18	1.582	3.854	567	72.4	8.2	40	1.320
106 RIE	11.75	1.526	3.869	562	70.2	8.0	28	1.500
Ref 9000	12.92	1.679	3.932	582	73.3	10.0	91	1.185

We have also applied nanoscale-texturing schemes on 4" polished Si wafers. Figure 16 shows IQE measurements on randomly RIE textured, control and wet-chemically polished Si solar cells. Randomly textured Cell (green line) was formed by depositing a thin (~ 5 nm) Cr film on Si. This island Cr film was then used as an etch mask for nanoscale texturing of top Si surface. Salient features of these measurements are listed below:

a) Highest efficiency has been obtained for the randomly textured solar cell,
b) Randomly textured cell has lower IQE in 300-700-nm spectral region than either the control, or chemically-textured cell, and
c) Randomly textured cell has higher IQE in 700-1200-nm spectral region than either the control, or chemically textured cell.

It is known that reactive ion etching techniques produce surface damage [15-18]. Various surface passivation techniques have been investigated in reducing RIE damage [15, 19]. For the solar cell devices shown in Fig. 16, surface passivation treatment consisted of a thin (~10 nm) thermally grown oxide film. The UV response of RIE cell fabricated using (green line) is lower than either the chemically-textured (black line), or the control cell (red line), we expect to improve IQE of RIE-textured cell by additional passivation treatments. We have also fabricated periodically textured solar cells. Figure 17 shows IQE measurements on a 1-D (period ~ 800 nm, green line) grating structure, for comparison results of control (red line) and wet-etched (black line) cell are also shown. The salient features of these measurements are:

a) Highest efficiency has been obtained for the RIE textured solar cell,
b) Periodically textured cell has slightly lower IQE in 300-400-nm spectral region than either the control, or chemically-textured cell, and
c) Periodically textured cell has higher IQE in 800-1200-nm spectral region than either the control, or chemically textured cell.

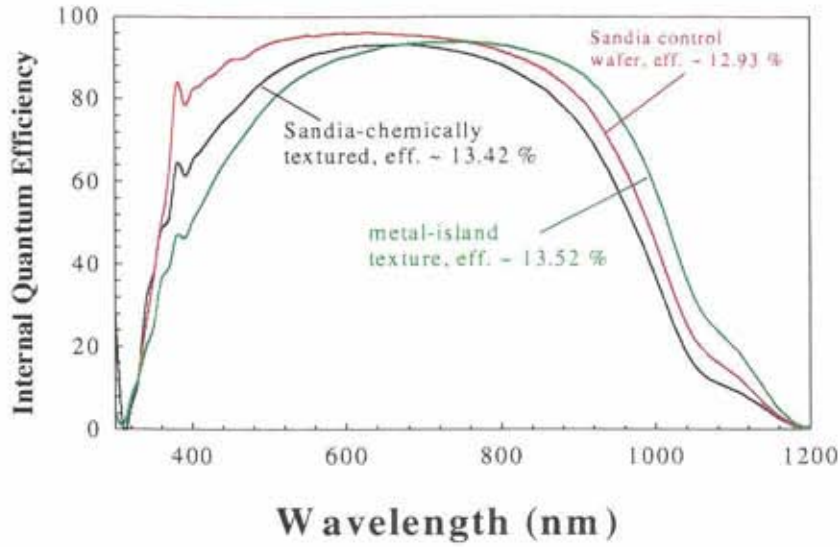

Figure 16 Internal Quantum efficiency measurements on randomly textured solar cells.

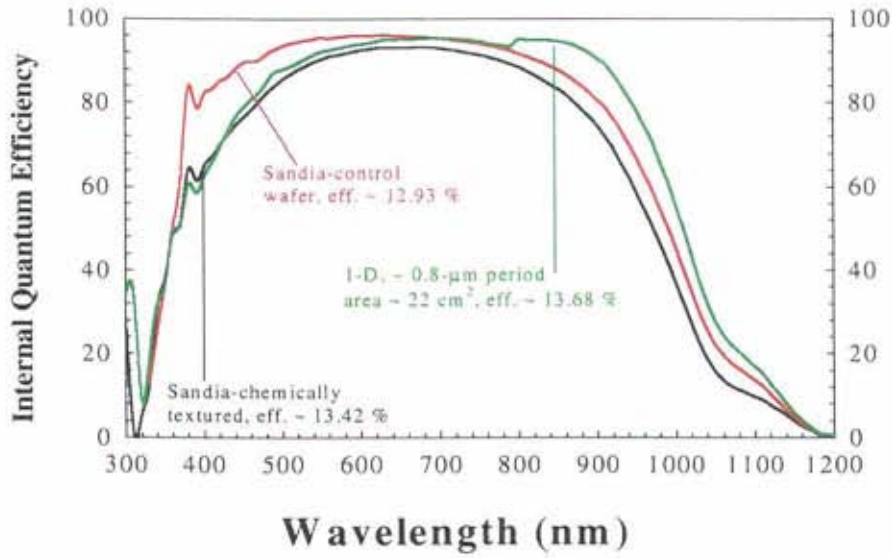

Figure 17 Internal Quantum efficiency measurements on 1-D periodically textured solar cells.

Comparison between random and periodic 1-D textured cells shows that there is less surface damage for periodical structures. Both 1-D and 2-D random structures show improved IQE in 700-1200-nm spectral region. The sharp increase in 1-D grating IQE at $\lambda \sim 800$ nm probably corresponds to an artifact of measurement, since λ=800 nm, the detector is changed for IR reflectance measurements. Overall it appears that grating cell has higher IQE in IR region. We expect this enhancement to be more pronounced for 2-D grating structures. For space solar cell applications, a comparison of random and periodic textures in IR range is more meaningful as shown in Fig. 18. It is seen that both random and periodic textures have produced similar IQE improvement. In 800-900-nm spectral range, 1-D grating is better than random

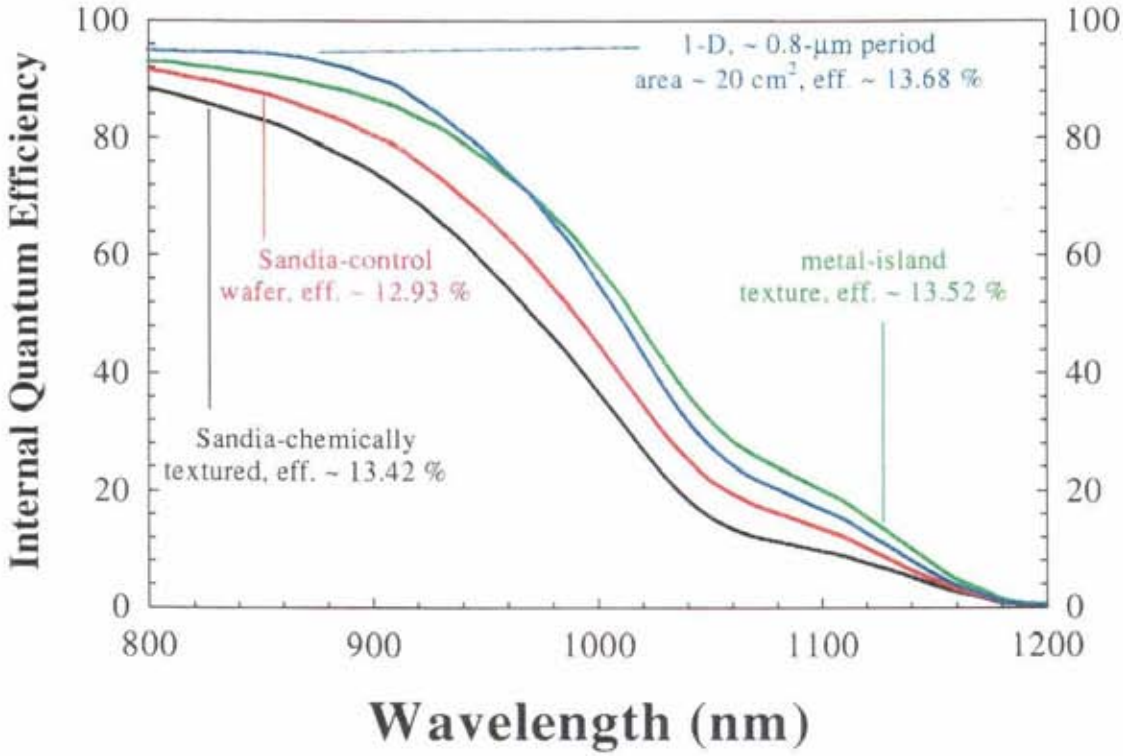

Figure 18 Internal Quantum efficiency measurements on random and periodically textured solar cells in 800-1100-nm spectral range.

structure. In 1000-1200-nm spectral range, random texture is superior in comparison with the 1-D grating structure. Both random and periodic textures provide improved performance in comparison with the control and conventionally wet-etched pyramidal surfaces.

5. Discussion of Results and Future Work

Reduced reflection of nanoscale random and periodic textures is due to light trapping in high aspect ratio λ/n type triangular profiles. These nanoscale textures not only have very large surface areas, but are also susceptible to the RIE process-induced surface damage. Therefore, commercial application of these textures requires an effective surface passivation scheme. Improved IQE in IR region despite

the lack of surface passivation is a good indicator of the potential of nanoscale texturing schemes in improving solar cell device performance. A grating surface has the potential for wavelength-selectivity, which is not easily accessible in randomly textured surfaces. Finally, these RIE texturing schemes are equally applicable to single and multi-crystalline Si surfaces.

5.a Random Texturing

Random texturing using TEOS oxide has performed very well, with the PECVD oxide results have not been as effective. We have investigated random texturing using thin ~ 5 nm island metal (Cr, or

Au, or Al) films. This approach shows significant promise, and had been applied in forming the randomly textured solar cell shown in Fig. 16. An island metal is vacuum-deposited in an e-beam sputtering system. For low-cost terrestrial Si solar cell applications, a room temperature, non-vacuum process is preferable. We will investigate a spin-on approach using metal-colloidal solutions [20]. This approach has been successfully applied in fabricating nanoscale random metal island surfaces in Raman scattering experiments.

5.b Periodic Texturing

We have investigated 1-D structures in detail. For coupling to non-polarized solar radiation, 2-D structures are required. 2-D patterns can be etched in Si either as holes, or posts [7]. Additional process variation is performance evaluation of round versus square hole, or post shape. Traditionally, gratings have been used either for optical coupling to waveguide modes [4], or for coupling to diffraction orders [21]. Our approach has been based on light trapping in high aspect ratio ~ λ/n linewidth textures. A comparison of Si solar cell devices based on both of these approaches will be carried out to assess performance.

5.c Surface Passivation

Key to successful implementation of nanoscale structures is their passivation. Large nanoscale surface areas without adequate passivation will negate enhanced absorption by electron-hole recombination. Surface passivation performance can be evaluated by lifetime measurements. We will investigate following surface passivation treatments:

a) wet-chemical etching of 25-50-nm top Si material followed by reactive-ion etching [15],
b) PECVD nitride films for passivation of etched areas [22],
c) Thermal and evaporated SiO_2 films followed by step a [23],
d) Al_2O_3 passivation [24], and
e) Hydrogen passivation [25-27].

We will investigate these passivation treatments to determine an optimum approach for improving the internal quantum efficiency of nanoscale-textured Si solar cells.

5.d Modeling of 1-D and 2-D Grating Structures

Most of the work reported here has described experimental characteristics of random and periodically textured surfaces. A basic physics understanding of the underlying physical optics is required. Grating theories have been developed for both rectangular [28] and triangular profiles [29-30]. Grating profile plays a critical role in determining its spectral response, the optimization in any spectral range requires a unique combination of grating pitch, linewidth, depth, and profile. We have acquired a commercially available software program GSOLVER, which is based on rigorous coupled wave analysis [30]. This program is applicable to any arbitrary 1-D, or 2-D grating profile. Some modeling work on 1-D grating structures has already been started. Figures 19-20 show zero and diffraction order spectral response in reflection and transmission for a 1.0-μm period, 0.3156-μm linewidth, and 1.25-μm deep rectangular profile grating respectively. It is seen from Fig. 19 that energy loss in zero-order corresponds to a slight increase in diffraction order intensity. However, Fig. 20 shows that most of the energy loss in reflection appears as gain in transmitted orders. The energy loss in zero-order transmission at $\lambda \sim 0.84$ & 1.16 μm appears as gain in first, second, and higher orders. The diffraction orders inside Si propagate at angles determined by grating equation. For space solar cell applications, it

is desirable to have maximum coupling into diffraction orders travelling parallel to the surface so that absorption takes place close to the junction. This modeling program will help us determine profiles required for highest quantum efficiencies.

5.e Radiation Damage Studies

For space solar cells, it is necessary to evaluate resistance to radiation damage of nanoscale textured surfaces. Since, we expect that light trapping takes place close to the surface, therefore, these cells are expected to be more resistance to surface damage. This has been demonstrated in vertical junction solar cells formed in (110) Si cells [31-32]. We plan to evaluate cell performance following radiation treatment.

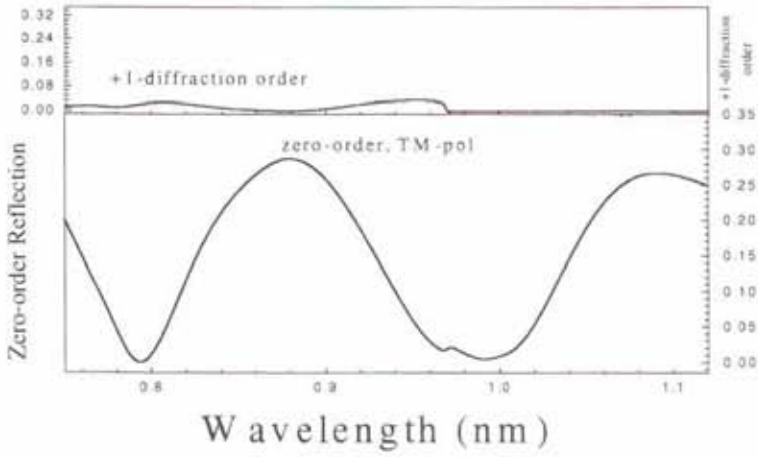

Figure 19 Normal incidence, spectral reflection from a 1000-nm period grating structure.

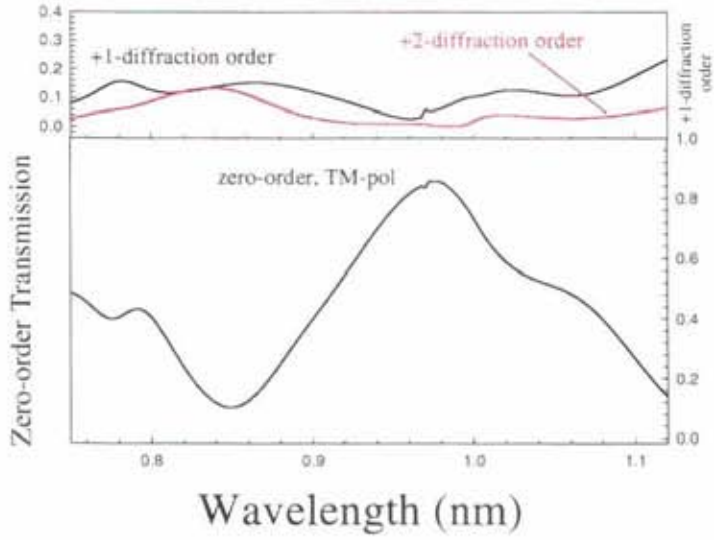

Figure 20 Normal incidence, spectral transmission from a 1000-nm period grating structure.

6. References

1. D. E. Aspness and A. A. Studna, Phys. Rev. **B 27**, 985 (1983).
2. B. O. Seraphin and A. B. Meinel in *Optical Properties of Solids*, North-Holland, Amesterdam (1974).
3. P. Campbell and M. A. Green, J. Appl. Phys. **62**, 243 (1987).
4. Ping Sheng, A. N. Bloch, and R. S. Stepleman, Appl. Phys. Lett. **43**, 579 (1983).
5. E. Yablonovitch, J. O. S. A. **72**, 899 (1982).
6. H. W. Deckmann, C. R. Wronski, H. Witzke, and E. Yablanovitch, Appl. Phys. Lett. **42**, 968 (1983).
7. Saleem H. Zaidi and S. R. J. Brueck, **26th** PVSC, 171 (1997).
8. Y. Tzeng and T. H. Lin, J. Electrochem. Soc. **134**, 2304 (1987).
9. J. I. Gittleman, E. K. Sichel, H. W. Lehman, and R. Widmer, Appl. Phys. Lett. **35**, 742 (1979).
10. H. G. Craighead, R. E. Howard, D. M. Tennant, Appl. Phys. Lett. **37**, 653 (1980).
11. H. Jansen, M. de Boer, B. Otter, and M. Elwensoek, Proc. IEEE MEMS-**95**, 88 (1995).
12. H. W. Deckmann and J. H. Dunsmuir, J. Vac. Sci. Technol. **B 1**, 1109 (1983).
13. Saleem H. Zaidi, An-Shyang Chu, and S. R. J. Brueck, J. Appl. Phys. **80**, 6997 (1996).
14. Saleem H. Zaidi and S. R. J. Brueck, J. Vac. Sci. Technol. **B 11**, 653 (1993).
15. S. W. Pang, D. D. Ratham, D. J. Silversmith, R. W. Mountain, and P. D. DcGraff, J. Appl. Phys. **54**, 3272 (1983).
16. G. S. Oehrlein and Y. H. Lee, J. Vac. Sci. Technol. **A 5**, 1585 (1987).
17. A. S. Yapsir, G. Fortune-Wiltshire, J. P. Gambino, R. H. Castle, and C. C. Parks, J. Vac. Sci. Technol. **A 8**, 2939 (1990).
18. J. M. Heddleson, M. W. Horn, and S. J. Fonash, J. Vac. Sci. Technol. **B 6**, 280 (1988).
19. K. H. Kwon, H. H. Park, K. S. Kim, C. Kim, and Y. K. sung, Jpn. J. Appl. Phys. **35**, pt 1, 1611 (1996).
20. G. Chumanov, K. Sokolov, B. W. Gregory, and T. M. Cotton, J. Phys. Chem. **99**, 9466 (1995).
21. C. Heine and R. H. Morf, Appl. Opt. **34**, 2476 (1995).
22. D. S. Ruby, W. L. Wilbank, C. B. Fleddermann, and J. I. Hanoka, Proc. **13th** EPSEC, 1412 (1995).
23. P. E. Greenbaum, J. Y. Gan, R. R. King, and R. M. Swanson, IEEE PVSC-**90**, 317 (1990), A. Aberie, Warta, J. Knobloch, B. Vob, **ibid** 233 (1990).
24. K. Jaeger and R. Hezel, IEEE PVSC-**85**, 1752 (1985).
25. W. Schmidt, K. D. Rasch, and K. Roy, IEEE PVSC-**82**, 537 (1982).
26. Z. Xu, B. Xia, and Y. Yang, IEEE PVSC-**87**, 1050 (1987).
27. Y. Saito, M. Aomori, and H. Kuwano, J. Appl. Phys. **81**, 754 (1997).
28. Ping Sheng, R. S. Stepleman, and R. N. Sanda, Phys. Rev. **B 26**, 2907 (1982).
29. D. H. Raguin and G. M. Morris, Appl. Opt. **32**, 1154 (1993).
30. M. G. Moharam and T. K. Gaylord, J. Opt. Soc. Amer. **72**, 1385 (1982).
31. D. H. walker and R. L. Statler, IEEE PVSC-**87**, 697 (1987).
32. J. Wohlgemuth and C. Wrigley, IEEE PVSC-**13**, 459 (1978).

Keith Matthei
GT Solar Technologies
472 Amherst Street
Nashua, NH 03063

Ed Henderson
Matrix Solar
P. O. Box 14740
Albuquerque, NM 87191-4740

Mike Nowlan
Spire Corporation
One Patriots Park
Bedford, MA 01810

Steve Hogan
Spire Corporation
One Patriots Park
Bedford, MA 01810

Dr. Juris Kalejs
ASE Americas,Inc.
Four Suburban Park
Billerica, MA 01821-3980

Dr. Michael Kardauskas
ASE Americas, Inc.
Four Suburban Park
Billerica, MA 01821-3980

Dr. Mark Rosenblum
ASE Americas, Inc.
Four Suburban Park
Billerica, MA 01821-3980

Dr. James Rand
AstroPower
Solar Park
Newark, DE 19716-2000

Dr. Bob Hall
AstroPower
Solar Park
Newark, DE 19716-2000

Dr. Chandra Khattak
Crystal Systems
27 Congress Street
Salem, MA 01970

Dr. Mohan Narayanan
Solarex Corporation
630 Solarex Court
Frederick, MD 21701

Dr. John Wohlgemuth
Solarex Corporation
630 Solarex Court
Frederick, MD 21701

Mr. Ted Ciszek
NREL
1617 Cole Blvd.
Golden, CO 80401-3393

Dr. Bhushan Sopori
NREL
1617 Cole Blvd.
Golden, CO 80401-3393

Dr. Jack Hanoka
Evergreen Solar, Inc.
211 Second Avenue
Waltham, MA 02154

Dr. Andrew Gabor
Evergreen Solar, Inc.
211 Second Avenue
Waltham, MA 02154

Ms. Theresa Jester
Siemens Solar Industries
P. O. Box 6032
Camarillo, CA 93011

Dr. Dan Meier
Ebara Solar, Inc.
811 Rt. 51 South
Large, PA 15025

Prof. Ajeet Rohatgi
Georgia Institute of Technology
777 Atlantic Drive
School of Electrical Engineering
Atlanta, GA 30332

Dr. Jeffrey Mazer
U. S. Department of Energy
Forrestal Bldg., EE-11
1000 Independence Ave., SW
Washington, D.C. 20585

Dr. Richard King
U. S. Department of Energy
Forrestal Bldg., EE-11
1000 Independence Ave., SW
Washington, D.C. 20585

Dr. Richard Swanson
SunPower Corporation
430 Indio Way
Sunnyvale, CA 94086

Dr. Richard King
Spectrolab, Inc.
12500 Gladstone Avenue
Sylmar, CA 91342-5373

Mr. Frank Ho
Tecstar, Inc.
15251 E. Don Julian road
City of Industry, CA 91745

0752 Dan Aiken, 6219
0752 David King, 6219
0752 Doug Ruby, 6219
0752 James Gee, 6219
0753 C.P. Cameron, 6218

0899 Technical Library (2)
R/A Desk for DOE/OSTI, 0619
Central Technical Files, 9018